Dyes and Pigments 82 (2009) 299–306

Contents lists available at ScienceDirect

Dyes and Pigments

journal homepage: www.elsevier.com/locate/dyepig

X-ray and molecular modelling studies of 4-[*N*-alkylamino]azobenzene dyes

Liang He [a,b,*], Ahmed El-Shafei [b], Harold S. Freeman [b], Paul Boyle [c]

[a] State Key Laboratory of Fine Chemicals, Dalian University of Technology, Dalian 116012, PR China
[b] Fiber and Polymer Science Program, North Carolina State University, Raleigh, NC 27695-8301, USA
[c] Department of Chemistry, North Carolina State University, Raleigh, NC 27695-8204, USA

ARTICLE INFO

Article history:
Received 29 November 2008
Received in revised form
17 January 2009
Accepted 21 January 2009
Available online 31 January 2009

Keywords:
Aminoazobenzene dyes
DFT calculations
Solvatochromism
X-ray diffraction
Polarizability
Asymmetric molecules

ABSTRACT

4-[*N*,*N*-Bisalkyl]amino-2′-chloro-4′-nitroazobenzenes were recrystallized from acetone in either triclinic or monoclinic cells with the space group *P*-1 or $P2_1/c$. The asymmetric unit cell of dyes having at least one *N*-cyanoethyl group contained two molecules that were symmetrically unequivalent. The aromatic rings in the azobenzene skeleton were essentially planar with respect to the plane of the azo group, although the C6–C1–N1–N2 torsion angle was 13.2° when the *N*,*N*-dicyanoethyl group was employed. X-ray studies were used as a basis for assessing the utility of nonlocal DFT calculations in predicting the equilibrium molecular geometry and solvatochromic properties of the compounds using MM3/ZINDO-S and the COSMO Solvation Model. Although B3LYP and PBE energy functionals were comparable in predicting bond lengths, PBE was slightly better than B3LYP in predicting torsion angles. Furthermore, the dipolarity/polarizability index (π^*) was the preferred solvent parameter for predicting the effects of solvents on λ_{max}.

1. Introduction

Aminoazobenzenes include a family of synthetic colorants known as disperse dyes. These dyes have very low water solubility making them suitable for adding colour to hydrophobic polymers. The first disperse dyes were used for dyeing cellulose acetate fibres [1] and since 1950, disperse dye production has increased significantly, following increases in synthetic fibre production based on polyethylene terephthalate [2]. Disperse dyes that are readily sublimable are used for transfer printing [3] and disperse dyes are also available that meet end-use applications requiring high sublimation fastness and light fastness [4–7].

While disperse dyes include anthraquinone, naphthalimide, naphthoquinone, methine and nitro systems [8], monoazo dyes derived from aromatic amines as coupling components and carbocyclic aromatic amines as diazo components constitute the types of greatest economic importance [9]. Monoazo disperse dyes cover the full colour spectrum, owing to the wide range of donor–acceptor systems (cf. Fig. 1). These dyes often exhibit solvatochromism, with increasing solvent polarity normally producing a bathochromic shift in λ_{max}. However, if the ground state of the dye is more polar than the excited state, the interaction of polar solvents with the ground state will be stronger than with the excited state, resulting in a hypsochromic shift [10].

Interestingly, there is no single parameter that precisely describes solvent polarity. In this regard, solvent polarity can be characterized by dipole moment (μ), which is a property of an individual molecule, and dielectric constant (ε) [11]. Dielectric constant is a measure of the effects of a substance on an electric field between two parallel and oppositely charged plates but it does not indicate how precisely solvent molecules are aligned around a solute. Solvent polarity and polarizability influence dielectric constants, but the arrangement of solvent molecules around a charged or polar solute should be very different from the arrangement of solvent molecules between two charged metal plates [12,13].

There have been many attempts to develop empirical parameters for solvent polarity that reflect the interaction of polar molecules with solutes and correlate better with results from chemical reactions [14]. While various scales have been developed based on the effects of solvents in model reactions [11], others are based on measurements of physical properties of solutes in a solvent. However, most scales are based on solvatochromism, the most cited of which are the Kosower Z scale which is based on the charge transfer absorption spectra of 1-ethyl-4-carbomethoxypyridinium iodide [13,15] and the E_T scale based on the spectrum of a pyridinium *N*-phenol betaine [14].

* Corresponding author. State Key Laboratory of Fine Chemicals, Dalian University of Technology, No. 158 Zhongshan Road, Dalian 116012, PR China. Tel./fax: +86 411 39893621.
E-mail address: lhedlut2002@yahoo.com.cn (L. He).

0143-7208/$ – see front matter © 2009 Elsevier Ltd. All rights reserved.
doi:10.1016/j.dyepig.2009.01.013

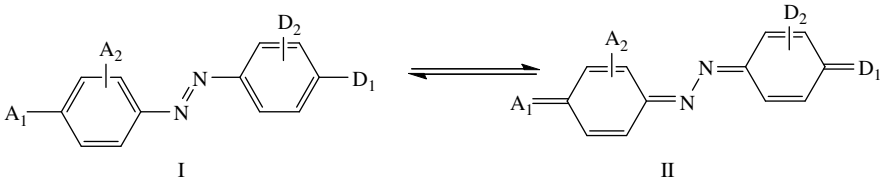

Fig. 1. Electron-delocalization in a monoazo donor (D)–acceptor (A) system (structure I).

Kamlet and co-workers developed a general polarity/polarizability index (π^*) to characterize the ability of a solvent to stabilize an ionic or polar species via its dielectric effect. The π^* values are based on the solvatochromic parameters of a significant number of dyes [16]. Also, Buncel and co-workers developed the π^*_{azo} scale based on the spectral properties of azo merocyanine dyes [17]. The effects of solvents on either a chemical reaction or an absorption spectrum could arise from the ability of a solvent to function as a hydrogen bond donor or acceptor. In this regard, α and β parameters were developed as measures of the ability of solvents to function as proton acceptors and proton donors, respectively [16,18]. Developments in the realm of optical communications, dynamic image processing, optical computing, and data storage have been receiving much attention recently. Hence, organic materials that have large non-linear optical (NLO) responses coupled with photoswitching are of significant importance. In this respect, there has been considerable research effort towards the design and synthesis of more efficient photon-maneuvering materials [19–25] for use in different optical devices. Studies of this type are of interest nowadays because organic chromophores based on donor–acceptor groups can furnish materials with promising NLO properties, which can be estimated from their hyperpolarizabilities [19,25,26]. The first hyperpolarizability (α') provides information about a substrate's potential to exhibit second order non-linear effects, such as second harmonic generation, sum of frequency generation, and parametric amplification [26].

Azo dyes having a wide range of donor and acceptor (D–A) groups and the potential to exhibit second order non-linear optical (NLO) properties have been synthesized, and it is known that the planarity of the azobenzene skeleton significantly contributes to the observed transmission effects and leads to enhanced optical activity [27–30]. Azobenzene homologs not only possess NLO properties but due to photo-induced *cis–trans* isomerisation, they also exhibit photoswitching which makes them useful for different technological applications such as LC displays, NLO materials and information storage devices [29].

The present paper reports results from studies towards the identification of molecular modelling methods suitable for predicting the equilibrium molecular geometry and hyperpolarizability of the title compounds (cf. Fig. 2). The effects of solvent polarity on λ_{max} was calculated using MM3/ZINDO-S via the COSMO Solvation Model [31] and the results compared to experimental data from single crystal X-ray analysis.

2. Experimental

2.1. Dye synthesis

The procedure employed is illustrated in the synthesis of 4-[*N*-ethyl-*N*-cyanoethyl]amino-2′-chloro-4′-nitroazobenzene (dye **1**).

Finely powdered $NaNO_2$ (1.7g, 23.6 mmol) was added slowly and with stirring to conc. H_2SO_4 (20 mL). The mixture was heated to 70 °C, held at this temperature for 10 min, and then cooled below 10 °C. 2-Chloro-4-nitroaniline (3.7g, 21.1 mmol) was added slowly to the solution of $NOHSO_4$ and the temperature was kept below 20 °C using an ice bath. The resulting solution was stirred at 10 °C for 1 h, and 10 g ice was added. The solution was then added dropwise to a solution of *N*-(2-cyanoethyl)-*N*-ethylaniline (3.68, 21.1 mmol) in HOAc (20 mL), stirred for 5 h at 10 °C, poured into water (1 L), adjusted to pH 6, and filtered. After drying, dye **1** was obtained (6.8 g, 90%), mp 129–130 °C.

2.2. X-ray diffraction

Single crystal formation was achieved by dissolving dye (0.5 g) in acetone (50 mL) at 23 °C (room temperature) and the resulting solution was covered with a Parafilm plastic containing pinholes and kept for 1 week, allowing slow evaporation of solvent.

2.2.1. Data collection and processing

The procedure employed is illustrated for the analysis of dye **1**.

A single crystal of dye **1** was mounted on a nylon loop using a small amount of Paratone N oil. All X-ray measurements were made on a Bruker-Nonius X8 Apex2 diffractometer at a temperature of 110 K. The unit cell dimensions were determined from a symmetry constrained fit of 9674 reflections with $4.94° < 2\theta < 71.44°$. The data collection strategy was a number of ω and φ scans which collected data up to 72.6° (2θ). The frame integration was performed using SAINT [32]. The resulting raw data were scaled and absorption corrected using a multi-scan averaging of symmetry equivalent data using SADABS [33].

2.2.2. Structure solution and refinement

The structures were solved by direct methods using the XS program [34]. Non-hydrogen atoms were obtained from the initial solution and the hydrogen atoms were introduced at idealized positions and were allowed to refine isotropically. The structural model was fit to the data using full matrix least-squares based on F^2. The calculated structure factors included corrections for anomalous dispersion from the usual tabulation. The structure was refined using the XL program from SHELXTL [35], and graphic plots were produced using the NRCVAX crystallographic program suite. Additional information and other relevant literature references can be found at http://www.xray.ncsu.edu. Cambridge Crystallographic

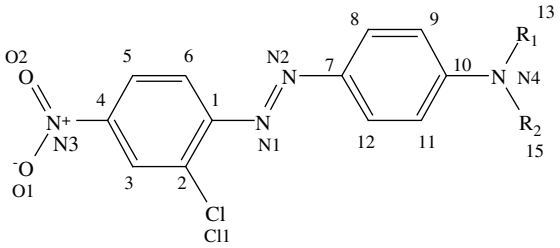

Dye **1** $R_1 = CH_2CH_2CN$, $R_2 = CH_2CH_3$
Dye **2** $R_1 = R_2 = CH_2CH_2CN$
Dye **3** $R_1 = R_2 = CH_2CH_2CH_3$

Fig. 2. Structures of dyes **1**–**3** employed in this investigation.

Database (CCD) listings 716116–716118 contain the supplementary crystallographic data for dyes **1**–**3**. This information can be obtained from www.ccdc.cam.ac.uk/data_request/cif.

2.3. Absorption spectra

Absorption maxima (λ_{max} values) were recorded in *n*-hexane, chloroform, toluene, methanol, ethanol, ethyl acetate, acetonitrile, tetrahydrofuran, acetone, DMF, and DMSO using a Varian Cary 3 UV–vis spectrophotometer. Absorption spectra were predicted using MM3/ZINDO-S implemented in CAChe 6.12.33 [36]. In this case, the effects of solvent on λ_{max} were accounted for by defining the dielectric constant for each solvent using MM3/ZINDO-S and the Solvation Model COSMO implemented in ZINDO.

2.4. Molecular modelling studies

DFT methods were used to predict equilibrium molecular geometry of dyes **1**–**3** including B3LYP energy functional with basis set 6-31G* (d, p), and PBE energy functional and DNP basis set. λ_{max} values for dyes **1**–**3** in different solvent polarities were calculated using MM3/ZINDO-S and the Solvation Model COSMO implemented in ZINDO. The calculations were performed on an Intel(R)Xeon CPU(5482) at 3.2 GHz with 3 GB of RAM.

3. Results and discussion

3.1. X-ray structures

X-ray data pertaining to *trans*-azobenzenes without *ortho*-substituents are available from the Cambridge Crystallographic Database (CCD, 2008) [37]. It is clear that such compounds are characterized by a significant degree of conjugation across the azobenzene system, as evidenced by the coplanarity of rings in the azobenzene moiety and shortening of the two N–C bonds associated with the coupler ring (Fig. 3). For the examined X-ray structures, the torsion angles for C6–C1–N1═N2 and C12–C7–N2═N1 are $<11.6°$, and the average bond length for C7–N2 and C1–N1 are 1.420 Å and 1.431, respectively, with the longer one associated with the diazo component. Moreover, the average bond lengths for C10–N4 and C4–N3 are 1.37 and 1.46 Å. This indicates that the mesomeric effect of the N4 lone pair is greater on the coupler ring.

In the present study, dyes **1**–**3** have a chloro group in the *ortho* position of the acceptor moiety and one would expect this feature to affect C–N bond lengths associated with the diazo component. However, the X-ray structure of dye **1** showed the same pattern reported for Fig. 1 structures without A_2D_2 groups [38]. In the dye **1** structure, the nitro group oxygen atoms are twisted only slightly out of the azobenzene plane (5–6°). Interestingly, results shown in

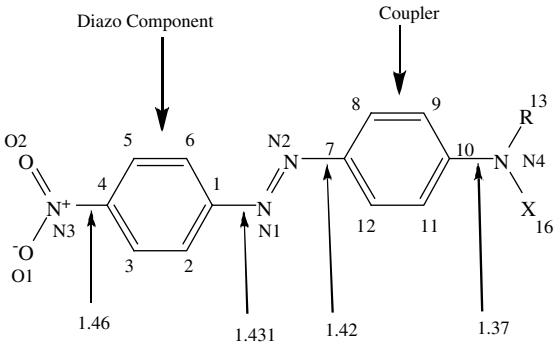

Fig. 3. Average bond lengths (Å) for *trans*-azobenzenes with D–A groups [37].

Fig. 4a show that dye **1** molecules occupying the unit cell are symmetrically in-equivalent. The unit cell for dye **2** also reflected symmetrically in-equivalent molecules, while that for dye **3**, which does not have an *N*-cyanoethyl group, contained symmetrically equivalent molecules (Fig. 4b). Fig. 5 shows the ORTEP drawing of molecules A and B in the asymmetric unit cell of dye **2** and the lower diagram in this figure shows their orientation in the unit cell, where the two molecules are chemically equivalent.

Dye **1** crystallizes in space group *P*-1 with two molecules, designated **1A** and **1B**, in the asymmetric unit. Both molecules reside on general positions. The aromatic portions of the molecules are largely planar as evidenced by the dihedral angles between the aryl groups C1–C6 and C7–C12. For **1A** this dihedral angle is 3.56(5)° while for **1B** it is 4.29(5)°. The NO_2 groups are twisted relative to the aryl group to which they are bonded by 1.62(7)° for **1A** and 0.70(6)° for **1B**. The dihedral angle between the mean molecular planes for **1A** and **1B** is 6.45°.

The conformations around the dialkylamino group are significantly different between molecules **1A** and **1B**. For instance, in **1A** the C9A–C10A–N4A–C15A torsion is −174.92(8)°; whereas in **1B** the C9B–C10B–N4B–C15B torsion is 20.93(12)°, indicating an almost 180° flip of the dialkylamino group relative to the proximal aryl group. The twist, as given by the dihedral angles of the dialkylamino group relative to the aryl group to which it is bonded, is considerably less in **1A**, with a value of 5.56(7)°, than in **1B** which has a value of 16.70(4)°. The greater twisting of the dialkylamino group correlates with slightly greater puckering of the amino group. Atom N4B is slightly more puckered (0.0641(9) Å) out of the plane formed by the coordinated carbon atoms than in **1A** where N4A is only 0.0054(9) Å out of the plane. The torsion angles for the *N*-ethyl groups in molecules **1A** and **1B** are roughly similar, with their absolute values differing (accounting for the different overall sense of the torsion) by 9.32°. The torsions for the *N*-cyanoethyl groups are, on the other hand, substantially different. The

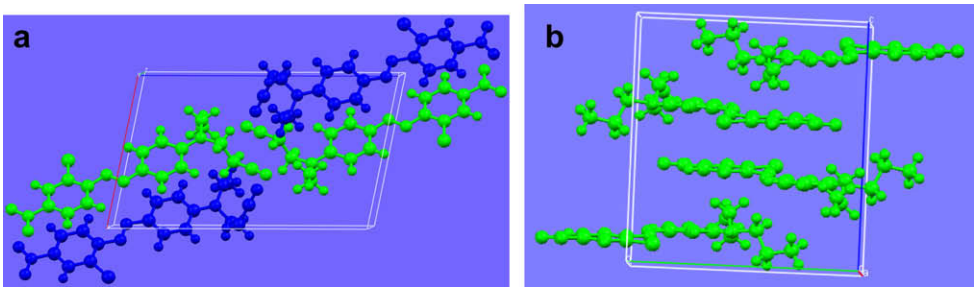

Fig. 4. Views of the dye 1 unit cell looking down the *b* axis (a), and dye 3 unit cell looking down the *b* axis (b).

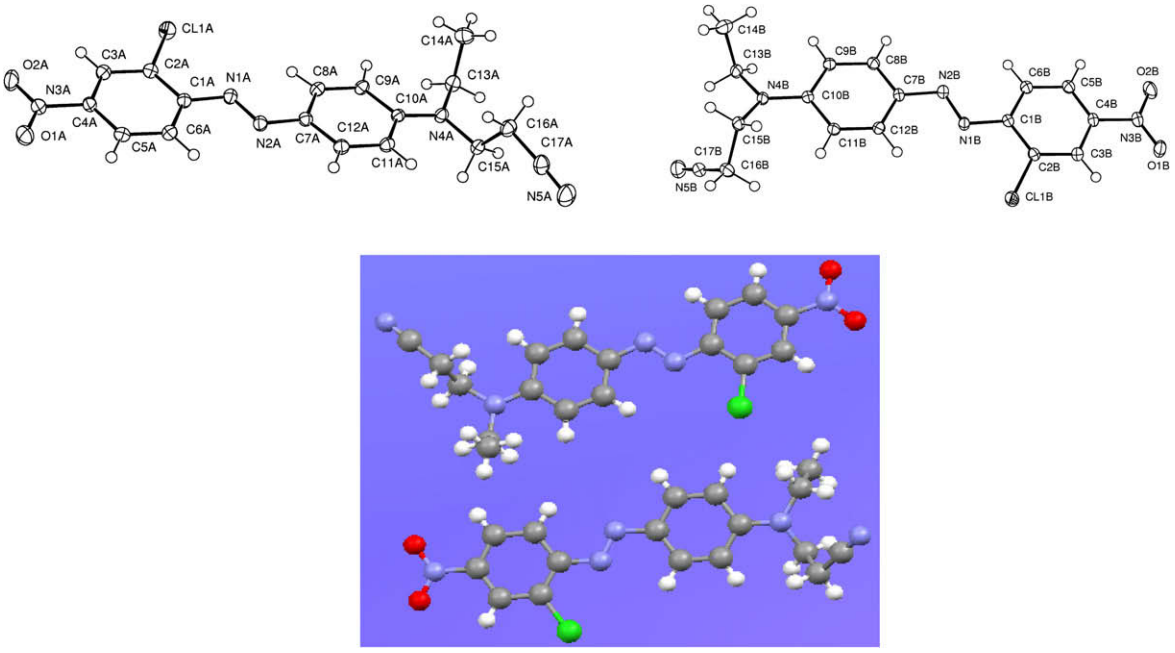

Fig. 5. ORTEP drawings of in-equivalent dye 1 molecules (A – top left, B – top right) showing numbering scheme and picture of type A and B molecules in the unit cell (lower diagram).

N4A–C15A–C16A–C17A torsion is 172.01(8)° while the N4B–C15B–C16B–C17B torsion is −61.30(11)°. This results in the *N*-ethyl group and the *N*-cyanoethyl group becoming *syn* relative to N4A in **1A** while in **1B** they are *anti*.

Dye **1** contains a number of hydrogen bond acceptor sites, but a paucity of classical hydrogen bond donors. As a consequence, its structure contains a number of unconventional C–H···X (X = Cl, O, N) hydrogen bonds. The C9B–H9B···Cl1A hydrogen bond crosses between **1A** and **1B** molecules in the asymmetric unit. The metrics for this interaction are H···Cl distance = 2.758(13) Å and the C9B-H9B···Cl1A angle = 142.2(9)°. There are also longer range C–H···Cl interaction between CL1B and H9A($2-x, 1-y, -z$) with a distance of 2.87 Å. There is a C–H···N hydrogen bond between N5B and H13A($x, y, 1+z$) with an H···N distance of 2.571(11) Å and C13A–H13A···N5B angle of 138.3(9)°. It is interesting to note that N5A, unlike N5B, does not participate in any C–H···N that could be reasonably described as hydrogen bonding interactions. Finally, both oxygen atoms (O2A and O1B) of the nitro groups are involved in C–H···O hydrogen bonds. The metrics for the O2A···H15C-C15B($1-x, 2-y, 1-z$) are O2A···H15C distance of 2.492(11) Å and the O2A···H15C–C15B angle is 166.0(10)°. Atom O1B is hydrogen bonded to two hydrogens. The metrics for these interactions are, O1B···H16D–C16B ($x, y, -1+z$): O···H distance 2.476(14) Å with the O1B···H16D–C16B angle 140.0(12)° and O1B···H16C-C16B($2-x$, $1-y$, $-z$) O···H distance of 2.576(12) Å with the O1B···H16C–C16B angle of 134.6(10)°.

The above results augment considerably the previous report of Reiss et al. [39] who described a hot solvent treatment method for β-modification of the crystal form of dye **1**. Also reported were powder diffractograms for dye **1** before and after thermal treatment. Similarly, the presence of non-classical intermolecular hydrogen bonds has been reported from a study of the X-ray structure of monoazo dye **4** [40].

Dye **2** also crystallizes in space group *P*-1 with two molecules, designated **2A** and **2B**, in the asymmetric unit. Both molecules reside on general positions. The aromatic portions of the molecules are slightly less planar than **1A** and **1B** as evidenced by the dihedral angles between the aryl groups C1–C6 and C7–C12. For **2A** this dihedral angle is 8.60(6)° while for **2B** it is 11.61(7)°. The NO_2 groups are twisted relative to the aryl group to which they are bonded by 9.04(6)° for 2**A** and 8.09(8)° for 2**B**. The dihedral angle between the mean molecular planes for 2**A** and 2**B** is 4.47°.

The chemical symmetry around the *N*,*N*-bis(cyanoethyl)-amino group of dye **2** is essentially C2, with the *N*-cyanoethyl groups assuming an *anti* conformation with regard to the molecular plane containing the amino nitrogen. The twist, as given by the dihedral angles of the dialkylamino group relative to the aryl group to which it is bonded, is 2.01(8)° and 1.71(8)° for **2A** and 5.56(7)°, respectively. The pucker values for the amino nitrogen are also similar, with the deviation of N4A from the C10A–C13A–C16A plane corresponding to 0.0199(12) Å while N4B deviates from the C1BA–C13B–C16B by 0.0144(12) Å.

Dye **2** is richer in hydrogen bond acceptor sites than is **1**, and has no classical hydrogen bond donor sites. As in **1**, there are number of unconventional C–H···X (X = N, O, Cl) hydrogen bonds in the structure of **2**. There is an intra-asymmetric unit C–H···Cl hydrogen bond between H9B and CL1A with an H···Cl distance of 2.655(17) Å. The C9B–H9B···CL1A angle is 132.3(13)°. The oxygen atoms from the nitro group on the **2A** molecule are involved in two C–H···O hydrogen bonds, while there are no comparable interactions involving molecule **2B**. The C12A–H12A···O1A ($2-x, 2-y, -z$) hydrogen bond has the following metrics: H12A···O1A distance 2.365(16) Å and C12A–H12A···O1A angle of 144.8(12)°. The other C–H···O hydrogen bond is C14B–H14D···O2A($2-x, 1-y, -z$) which has the following metrics: H14D···O2A distance is 2.496(16) Å and a C14B–H14D···O2A angle of 145.3(12)°. The closest approach to

Table 1
Different types of C–H···N intermolecular interactions of the cyano nitrogen-atom in dye **2**.

C–H···N	H···N (Å)	C–H···N (°)	Symmetry operation
C9A–H9A···N6A	2.475(16)	173.4(12)	$2-x, 2-y, 1-z$
C16B–H16D···N5A	2.522(15)	146.3(12)	$1-x, 2-y, 1-z$
C13A–H13B···N6B	2.540(15)	147.8(11)	$1-x, 2-y, 1-z$
C16A–H16A···N5B	2.627(15)	129.7(12)	$x, -1+y, z$

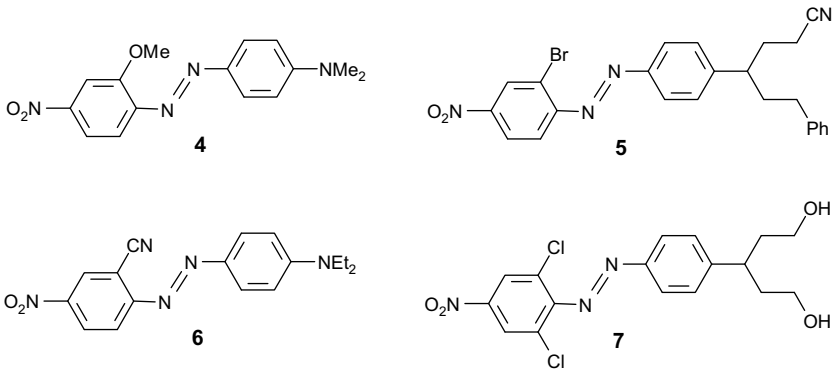

Fig. 6. Structures of dyes **4**–**7** employed in related studies.

the nitro oxygen atoms on **2B** is greater than 2.65 Å (to H14B ($1 - x$, $1 - y$, $-z$)).

The cyano nitrogens are involved in a number of C–H···N intermolecular interactions. The values are given in Table 1. The shortest H···N distance corresponds to the most linear C–H···N angle, as would be expected for an sp hybridized nitrogen. In general, as the interaction angle decreases, the H···N contact distance increases.

Table 2
Summary of crystal data for dyes **1**–**3**.

Data points	Dye 1	Dye 2	Dye 3
Formula	$C_{17}H_{16}ClN_5O_2$	$C_{18}H_{15}ClN_6O_2$	$C_{18}H_{21}ClN_4O_2$
Formula weight, g/mol	357.80	382.81	360.84
Crystal dimensions, mm	0.40 × 0.40 × 0.20	0.30 × 0.23 × 0.23	0.34 × 0.24 × 0.24
Crystal color and habit	Red prism	Red prism	Intense red prism
Crystal system	Triclinic	Triclinic	Monoclinic
Space group	*P*-1	*P*-1	$P2_1/c$
Temperature, K	110	110	110
a, Å	9.7522(4)	8.1005(4)	10.3458(7)
b, Å	10.8685(5)	11.8989(5)	12.8937(9)
c, Å	16.3399(8)	19.7645(9)	13.8273(10)
α,°	98.450(3)	75.020(2)	90.00
β,°	100.194(2)	84.052(2)	92.824(3)
γ,°	95.852(2)	73.444(2)	90.00
V, Å^3	1671.42(13)	1763.08(14)	1842.3(2)
Number of reflections to determine final unit cell	9674	9967	9936
Min and max 2θ for cell determination, °	0.0, 0.0	4.676, 66.33	4.32, 57.16
Z	4	4	4
F(000)	744	792	760
ρ, g/cm	1.422	1.442	1.301
λ, Å, Mo Kα	0.71070	0.71070	0.71070
μ (cm^{-1})	0.250	0.244	0.226
Diffractometer type	Bruker-Nonius X8 Apex2	Bruker-Nonius X8 Apex2	Bruker-Nonius X8 Apex2
Scan type (s)	Omega and phi scans	ω and ϕ scans	ω and ϕ scans
Max 2θ for data collection, °	72.6	67.56	59.14
Measured fraction of data	0.981	0.975	0.995
Number of reflections measured	97007	46974	59747
Unique reflections measured	15872	13815	5149
R_{merge}	0.0371	0.0356	0.0467
Number of reflections included in refinement	15872	13815	5149
Cut off Threshold Expression	$>2\sigma$ (*I*)	$>2\sigma$ (*I*)	$>2\sigma$ (*I*)
Structure refined using	Full matrix least-squares using F^2	Full matrix least-squares using F^2	Full matrix least-squares using F^2
Weighting scheme	Calc $w = 1/[\sigma^2(Fo^2) + (0.0617P)^2 + 0.0813P]$ where $P = (Fo^2 + 2Fc^2)/3$	Calc $w = 1/[\sigma^2(Fo^2) + (0.0701P)^2 + 0.0000P]$ where $P = (Fo^2 + 2Fc^2)/3$	Calc $w = 1/[\sigma^2(Fo^2)+(0.0633P)^2 + 0.2618P]$ where $P = (Fo^2 + 2Fc^2)/3$
Number of parameters in least-squares	579	607	310
R_1	0.0423	0.0472	0.0419
wR_2	0.1090	0.1200	0.1097
R_1 (all data)	0.0711	0.0774	0.0612
wR_2 (all data)	0.1215	0.1357	0.1200
GOF	1.078	1.047	1.076
Maximum shift/error	0.002	0.001	0.001
Min and max peak heights on final ΔF map (e$^-$/Å)	−0.377, 0.500	−0.339, 0.406	−0.364, 0.512

Where: $R_1 = \Sigma(|F_o| - |F_c|)/\Sigma F_o$; $wR_2 = [\Sigma(w(F_o^2 - F_c^2)^2)/\Sigma(wF_o^4)]^{1/2}$; GOF = $[\Sigma(w(F_o^2 - F_c^2)^2)/(\text{No. of reflections} - \text{No. of parameters})]^{1/2}$.

Table 3
Comparison of data from X-ray analysis and calculations using dyes **1–3**.

Dyes	Bond lengths (Å)												Torsion angles (°)					
	N1–N2			C10–N4		C7–N2		C1–N1		C4–N3			C12–C7–N2–N1			C6–C1–N1–N2		
	X-ray	Calc.[c]	Calc.[d]	X-ray	Calc.[c]	X-ray	Calc.[c]	Calc.[d]	X-ray	Calc.[c]	Calc.[d]	X-ray	Calc.[c]	Calc.[d]	X-ray	Calc.[c]	Calc.[d]
1A[a]	1.268	1.266	1.280	1.373	1.389	1.401	1.391	1.395	1.408	1.409	1.404	1.475	1.470	1.475	−1.03	1.43	−0.242	−1.52	3.11	0.848
1B[a]	1.268	1.266	1.280	1.372	1.389	1.403	1.391	1.395	1.372	1.409	1.404	1.459	1.470	1.475	6.26	1.43	−0.242	−2.39	3.11	0.848
2A[b]	1.271	1.22	1.278	1.374	1.416	1.404	1.415	1.396	1.414	1.418	1.403	1.463	1.462	1.476	−4.22	1.04	1.615	13.20	2.62	7.188
2B[b]	1.268	1.22	1.278	1.374	1.416	1.404	1.415	1.396	1.414	1.415	1.415	1.463	1.462	1.476	−4.22	1.04	1.615	−10.26	2.62	7.188
3	1.270	1.270	1.284	1.358	1.38	1.391	1.391	1.388	1.418	1.407	1.401	1.465	1.467	1.472	−5.14	0.92	0.982	1.90	−0.63	−2.44

[a] Symmetrically in-equivalent molecules.
[b] Symmetrically in-equivalent molecules.
[c] Using B3LYP energy functional and basis set 6-31G*(d, p).
[d] Using PBE energy functional and DNP basis set.

These results correlate well with data reported for other monoazo dyes giving a triclinic system and *P*-1 space group, an example of which is dye **4** (Fig. 6). Like *ortho*-chloro-substituted dyes **1** and **2** *ortho*-methoxy-substituted dye **4** gave crystals characterized by pairs of asymmetric molecules arranged anti-parallel within the unit cell [40]. In addition, the three dyes have N=N, C–NO_2, and C–N(R_1R_2) bond lengths that differ by less than 0.01 Å.

Dye **3** crystallizes in space group $P2_1/c$ with one molecule in the asymmetric unit. The aromatic portions of the molecule are largely planar, as evidenced by the dihedral angle of 4.02(1)° between the aryl groups C1–C6 and C7–C12. The NO_2 group is twisted relative to the aryl group by 5.80(2)°. The *N*,*N*-dipropylamino group is twisted slightly out of the C7–C12 plane by 10.75(2)°. The amino nitrogen sits 0.0291(13) Å out of the plane formed by C10, C13, and C16.

There are considerably less opportunities for hydrogen bonding offered by dye **3** than in dyes **1** and **2**. Only one C–H···O interaction, involving C18, H18A, and O1 ($1 + x$, $-1 + y$, z) can reasonably be described as an unconventional hydrogen bond. The metrics for this interaction are: the H···O distance = 2.597(18) Å and the C–H···O angle is 147.5(13)°. There is also a long range C–H···Cl ($-x$, $2 - y$, $-z$), interaction with an H···Cl distance of 2.939 Å, which maybe an attractive interaction. The interaction lies across a crystallographic inversion center, and therefore there is a symmetry equivalent Cl···H–C interaction to form an eight-membered ring.

Table 2 shows a summary of the X-ray data for dyes **1–3**, where it can be seen that the two dyes bearing at least one cyanoethyl group (dyes **1** and **2**) are characterized by a *P*-1 space group and the triclinic space group. Dye **3** on the other hand has a $P2_1/c$ space group and a monoclinic crystal system. All three dyes have the same number of molecules ($Z = 4$) per unit cell, and their molecular volume increases in the order dye **1** < dye **2** < dye **3**.

The present results are also interesting in the light of X-ray data published for other structurally related donor–acceptor monoazo dyes **5–7**. Like dye **3**, *ortho*-bromo-substituted azo dye **5** (C.I. Disperse Red 183) gave a monoclinic crystal system characterized by a $P2_1/c$ space group [41]. As would be expected, the bromo group caused a significantly larger C6–C1–N1–N2 dihedral angle (28° versus 1.90° for dye **3**). *ortho*-Cyano-substituted dye **6** gave crystals characterized by a PT space group, head-to-tail dimers forming a column structure in the unit cell, and ~3.5 Å spacings between molecules and dimers [42]. Dye **7** (C.I. Disperse Brown 1), which has chloro groups in both *ortho*-positions of the diazo components, gave a crystal structure having a C6–C1–N1–N2 dihedral angle of 45.5°, anti-parallel interlayer π–π stacking, and strong intermolecular H-bonding from OH groups [43].

3.2. DFT calculations

Table 3 provides a comparison of results from X-ray analysis and DFT calculations for key bond lengths and torsion angles of dyes **1–3**. Both dyes **1** and **2** have two symmetrically in-equivalent

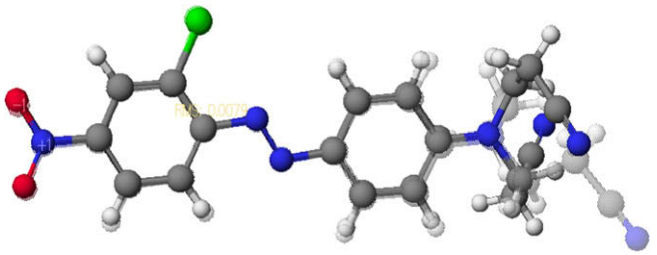

Fig. 7. X-ray crystal structure of dye 2 (solid) super imposed on the calculated equilibrium molecular geometry of dye 2 (shaded) using B3LYP energy functional and the basis set 6-31G*(d, p).

Table 4
Experimental and calculated λ_{max} values for dyes **1**–**3** in various solvents.

Solvent	λ_{max} (nm)					
	Dye **1**		Dye **2**		Dye **3**	
	Experimental	Experimental	Experimental	Calc.[b]	Experimental	Calc.[b]
n-Hexane	446	467	–[a]	–[a]	475	476
Chloroform	469	488	437	474	515	506
Toluene	466	473	445	461	499	484
Methanol	475	512	451	494	509	541
Ethanol	482	510	456	492	512	538
Ethyl acetate	476	492	456	478	506	512
Acetonitrile	482	512	457	493	515	542
Tetrahydrofuran	482	496	458	481	511	518
Acetone	485	508	461	490	515	536
DMF	501	512	475	493	527	542
DMSO	510	513	487	494	534	544

[a] Insoluble.
[b] From MM3/ZINDO-S calculations.

molecules in the unit cell designated **1A**, **1B**, **2A** and **2B**, respectively. Although the bond lengths of the symmetrically in-equivalent molecules were somewhat equal, the torsion angles varied considerably (Table 3, X-ray data). Results from DFT calculations were consistent with X-ray data in describing the positive mesomeric effect generated by the lone pair on the tertiary amino nitrogen atom attached to the coupler. Specifically, it was shown that the four C–N bond lengths varied in the order C10–N4 < C7–N2 < C1–N1 < C4–N3. Although B3LYP and PBE energy functionals were comparable in reliability for predicting bond lengths, PBE was better than B3LYP in predicting torsion angles in the case of dye **2**, which has an atypical torsion angle for C6–C1–N1–N2. Fig. 7 shows the X-ray crystal structure (solid) superimposed on the calculated structure (shaded) of dye **2** with an RMS = 0.0078, which further confirms the accuracy of the B3LYP functional in predicting the correct equilibrium molecular geometry.

Table 4 provides a summary of the effects of different solvents on the λ_{max} of dyes **1**–**3**. It is clear that λ_{max} increased with increasing solvent polarity, with the lowest experimental values observed in hexane and the highest in DMSO. Generally, the combination of MM3 and ZINDO-S gave higher calculated λ_{max} values than those measured. In this regard, the model over-estimated the effects of methanol and ethanol, predicting significantly higher λ_{max} values than those obtained experimentally. Otherwise, the model reflected the expected increase in λ_{max} with increasing solvent polarity. Table 5 shows correlation coefficients for dyes **1**–**3** in different solvents using three established solvent polarity parameters. The solvent polarity descriptor that best described the solvatochromism of dyes **1**–**3** was the dipolarity/polarizability index (π^*). Fig. 8 shows the correlation between the changes in λ_{max} of dye **3** upon changing the solvent polarity and reflects a very good R^2 value. A somewhat lower R^2 value was found in the case of dye **1**

Table 5
Correlation coefficients between λ_{max} of dyes **1**–**3** at different solvent polarities and solvent polarity parameters.

Solvent parameters	Correlation coefficient (R^2)		
	Dye 1 Experimental	Dye 2 Experimental	Dye 3 Experimental
Dipole moment (μ)	0.724	0.583	0.670
Dipolarity/polarizability index (π^*)	0.902	0.760	0.952
Dielectric constant (ε)	0.628	0.556	0.531
α	0.003	0.082	0.0008
β	0.684	0.563	0.520

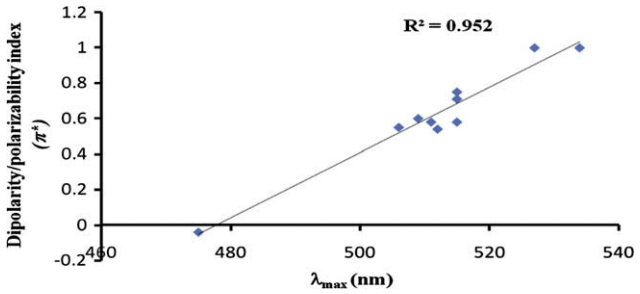

Fig. 8. Correlation of change in λ_{max} and solvent dipolarity/polarizability index (π^*) for dye **3**.

and a modest correlation was observed for dye **2**; although the value is still much better than those found using (μ) and (ε). Since the excited states of dyes **1**–**3** are more polar than their ground states, one should expect the more polar solvents to interact more strongly with the excited state of these dyes leading to a smaller HOMO–LUMO gap and a bathochromic shift.

4. Conclusions

Preparation of single crystals of the title dyes led to the determination of crystal structures for three 2′-chloro-4′-nitro-4-*N*,*N*-bisalkylaminoazobenzene dyes. The results suggest that the presence of cyanoethyl groups influenced the crystal system, space group, and whether equivalent or in-equivalent molecules are obtained in the asymmetric unit. It has also been shown that DFT calculations employing B3LYP and PBE energy functionals are effective in predicting the degree of electron-delocalization for aminoazobenzene dyes, in that the results are comparable to experimental data derived from single crystal X-ray analysis. With regard to predicting torsion angles, PBE was slightly more effective than B3LYP. Results from theoretical experiments aimed at establishing a correlation between λ_{max} and solvent polarity suggest that the dipolarity/polarizability index (π^*) is the preferred solvent parameter for predicting solvent effects.

References

[1] Fourness RK. The disperse dyes – their development and application. Journal of the Society of Dyers and Colourists 1956;72:513–27.
[2] Zollinger H. Color chemistry: synthesis, properties and application of organic dyes and pigments. 3rd ed. Zürich: Wiley-VCH; 2003.
[3] Moore NL. Heat-transfer printing a review of the literature. Journal of the Society of Dyers and Colourists 1974;90:318–25.

[4] Reife A, Freeman HS. Dyes for polyester: disperse dyes. Chimica Oggi 2007;25(4):38–41.
[5] Lampe T, Neumayer P, Roggenbach W. Alterung von textilwerkstoffen im kraftfahrzeug. Teil I: Beanspruchung und prüfverfahren. Melliand Textilberichte 1992;73:402–6.
[6] Ulbrich KH. Alterung von textilien im kraftfahrzeug. Teil II: Einfluβ der faserwerkstoffe. Melliand Textilberichte 1992;73:406–10.
[7] Vonhone P, Stuck J. Alterung von textilwerkstoffen im kraftfahrzeug. Teil III: Einfluβ der farbstoffe. Melliand Textilberichte 1992;73:411–6.
[8] Muller C. Disperse dyes. Chimia (Aarau) Supplement 1968:69.
[9] Hunger K. Industrial dyes: chemistry, properties, applications. 3rd ed. Weinheim: Wiley-VCH; 2003.
[10] Zollinger H. Color chemistry: synthesis, properties and application of organic dyes and pigments. 2nd ed. Weinheim: VCH; 1991.
[11] Felix A. Carroll, perspectives on structure and mechanism in organic chemistry. New York: Brooks/Cole Publishing Company; 1998.
[12] Riddick JA, Bunger WB, Sakano TK. Organic solvents: physical properties and methods of purification. In: Techniques of Chemistry. 4th ed., vol. II. New York: Wiley-Interscience; 1986.
[13] Kosower EM. An introduction to physical organic chemistry. New York: John Wiley & Sons, Inc.; 1968.
[14] Reichardt C. Solvents and solvents effects in organic chemistry. 2nd ed. Weinheim: VCH; 1988.
[15] Kosower EM. The effect of solvent on spectra. I. A new empirical measure of solvent polarity: *Z*-values. Journal of the American Chemical Society 1958;80:3253–60.
[16] Kamlet MJ, Abboud JLM, Abraham MH, Taft RW. Linear solvation energy relationships. 23. A comprehensive collection of the solvatochromic parameters, pi*,alpha, and beta, and some methods for simplifying the generalized solvatochromic equation. The Journal of Organic Chemistry 1983;48:2877–87.
[17] Buncel E, Rajagopal S. Solvatochromism and solvent polarity scales. Accounts of Chemical Research 1990;23:226–31.
[18] Marcus Y. The properties of organic liquids that are relevant to their use as solvating solvents. Chemical Society Reviews 1993;22:409–16.
[19] Kanis DR, Ratner MA, Marks TJ. Design and construction of molecular assemblies with large second-order optical nonlinearities. Quantum chemical aspects. Chemical Reviews 1994;94:195–242.
[20] Williams DJ. Non-linear optical properties of organic materials. Thin Solid Films 1992;216:117–22.
[21] Mendes PJ, Prates Ramalho JP, Candeias AJE, Robalo MP, Garcia MH. Density functional theory calculations on η^5-monocyclopentadienylnitrilecobalt complexes concerning their second-order nonlinear optical properties. Journal of Molecular Structure: Theochem 2005;729:109–13.
[22] Cerqueira NMFSA, Oliveira-Campos AMF, Coelho PJ, Melo de Carvalho LH, Samat A, Guglielmetti R. Synthesis of photochromic dyes based on annulated coumarin systems. Helvetica Chimica Acta 2005;85:442–50.
[23] Costa SPG, Griffiths J, Kirsch G, Oliveira-Campos AMF. Synthesis of thieno[2,3-*d*]thiazole derived dyes with potential application in nonlinear optics. Anales de Quimica International Edition 1998;94:186–8.
[24] Barachevsky VA, Oliveira-Campos AMF, Stebunova LV, Chudinova GK, Avakyan VG, Maslianitsin IA, et al. Thienothiazole azo dyes: photochromism and nonlinear behavior. Zhurnal Nauchnoi I Prikladnoi Fotografii (Russia) 2002;47:4–8.
[25] Raposo MMM, Sousa AMRC, Fonseca AMC, Kirsch G. Thienylpyrrole azo dyes: synthesis, solvatochromic and electrochemical properties. Tetrahedron 2005;61:8249–56.
[26] Prasad PR, Williams DJ. Introduction to nonlinear optical effects in molecules and polymers. New York: Wiley-Interscience; 1991.
[27] Jeewandara AK, Nalin de Silva KM. Are donor–acceptor self organised aromatic systems NLO (non-linear optical) active? Journal of Molecular Structure: Theochem 2004;686:131–6.
[28] Towns AD. Developments in azo disperse dyes derived from heterocyclic diazo components. Dyes and Pigments 1999;42:3–28.
[29] Yesodha SK, Sadashiva Pillai CK, Tsutsumi N. Stable polymeric materials for nonlinear optics: a review based on azobenzene systems. Progress in Polymer Science 2004;29:45–74.
[30] Åstrand P-O, Sommer-Larsen P, Hvilsted S, Ramanujam PS, Bak KL, Sauer SPA. Five-membered rings as diazo components in optical data storage devices: an ab initio investigation of the lowest singlet excitation energies. Chemical Physics Letters 2000;325:115–9.
[31] Klamt A, Schuurmann G. COSMO: a new approach to dielectric screening in solvents with explicit expressions for the screening energy and its gradient. Journal of the Chemical Society Perkin Transactions 2 1993:799–805.
[32] Bruker-Nonius. SAINT version 7.34A. Madison, WI 53711, USA: Bruker-Nonius; 2006.
[33] Bruker-Nonius. SADABS version 2.10. Madison, WI 53711, USA: Bruker-Nonius; 2004.
[34] Bruker-AXS, XS version 6.12, Bruker-AXS, Madison, WI 53711, USA.
[35] Bruker-AXS, XL version 6.12, Bruker-AXS, Madison, WI 53711, USA.
[36] CAChe, Fujitus, Oxford Molecular Group, Box 4003, Beaverton, OR 97076.
[37] Cambridge crystallographic Database (CCD, 2008).
[38] McIntosh SA, Freeman HS, Singh P. X-ray crystal structure of the dye 4(N,*N*-bis-(â-hydroxyethyl)amino)azobenzene. Dyes and Pigments 1991;17:1–10.
[39] Reiss E, Zeiler M, Mäder T. East German patent DD131652; 1978.
[40] Yang W, You XL, Zhong Y, Zhang DC. The crystal structure of 4-[(2-methoxy-4-nitro-phenylazo)-phenyl]-dimethylamine. Dyes and Pigments 2007;73:317–21.
[41] Główka ML, Ołubek Z. 2′-Bromo-4-[*N*-(2-cyanoethyl)-*N*-(2-phenylethyl)-amino-4′-nitroazo-benzene. Acta Crystallographica 1994;C50:458–60.
[42] Maginn SJ, Bullock JF, Docherty R. The solid state structures of donor-acceptor azobenzenes. Dyes and Pigments 1993;23:159–78.
[43] Seo J, Jo WJ, Choi G, Park KM, Lee SS, Lee JS. X-ray crystal structure of C.I. disperse Brown 1. Dyes and Pigments 2007;72:327–30.